IAES International Journal of Robotics and Automation (IJRA)
Vol. 15, No. 3, September 2026, pp. 597~606
ISSN: 2722-2586, DOI: 10.11591/ijra.v15i3.pp597-606

Performance assessment of fractional order PID control for a 2DOF flexible joint robotic manipulator under various operating conditions

Ahmed Alkamachi, Ali Hussien Mary
Mechatronics Engineering Department, Al-Khwarizmi College of Engineering, University of Baghdad, Baghdad, Iraq

Article Info

Article history:

Received Mar 20, 2026
Revised Jul 29, 2026
Accepted Aug 6, 2026

Keywords:

Fractional order PID
Flexible joint manipulator
Nonlinear robotic systems
Particle swarm optimization
Sliding mode control

ABSTRACT

Flexible joint robot manipulators (FJM) exhibit high nonlinear dynamics and coupling effects, which make their control a challenging task. This paper proposes a fractional order PID (FOPID) cascade control strategy for a 2DOF FJM. The controller performance is compared with that of a sliding mode controller (SMC) under identical operating conditions. Both controllers' parameters are optimally tuned using the particle swarm optimization (PSO) algorithm to ensure a fair performance evaluation. The proposed control consists of an inner loop that regulates motor dynamics and an outer loop that ensures accurate link position tracking. Additionally, a gravity compensator is integrated to improve control efficiency by reducing the nonlinear load on the controller. Both controllers are evaluated under nominal conditions, external disturbances, and variable payloads. Numerical results show a performance trade-off: under nominal conditions, FOPID achieved superior tracking performance (ITAE = 0.1165 for link 1) compared to SMC (ITAE = 0.2423), while SMC provided a smooth, zero-overshoot response and consumed much less actuator energy (ISCE = 23.35 vs. FOPID's 154.78). Furthermore, when subjected to a severe 1.0 N.m external disturbance, FOPID showed superb robustness by maintaining an ITAE of 0.178, whereas SMC suffered severe performance degradation. These findings illustrate the trade-offs between energy efficiency and robust precision in FJM control.

Corresponding Author:

Ahmed Alkamachi
Mechatronics Engineering Department, Al-Khwarizmi College of Engineering, University of Baghdad
Al-Jadriya, Karrada, Baghdad, Iraq
Email: ahmed78@kecbu.uobaghdad.edu.iq

1. INTRODUCTION

Flexible joint manipulators (FJMs) have attracted considerable interest due to their light weight structure, low energy consumption, and suitability for high-speed automated applications. However, the presence of flexible joint introduces strong nonlinearities, coupling effects, and complex dynamics, making controller design challenging [1], [2]. FJMs are growingly employed in light weight industrial robotic arms, participated robots, and automated manufacturing and assembly systems that require low weight, energy efficiency, and safe interaction. Recent studies have proposed advanced vibration suppression and trajectory tracking techniques for FJM to improve their stability and tracking performance under nonlinear dynamics, disturbances, and uncertainties [3], [4]. Classical PID based controllers are widely used due to their simplicity and ease of implementation, and they have been applied to different robotic systems [5], [6]. Nevertheless, their performance is often degraded when dealing with nonlinear systems such as FJMs. To overcome these limitations, researchers developed advanced control techniques. Neural network based and adaptive control methods have been employed to estimate system uncertainties and improve tracking performance [7]–[9]. Adaptive fuzzy and learning based control methods have been also proposed to improve robustness and compensate for model uncertainties [10], [11]. Model based approaches such as linear parameter varying (LPV) methods have also been introduced in [12] to simplify nonlinear system dynamics. Fuzzy logic based control considered another important direction, where it has been used for state feedback control and online tuning of controller parameters [13], [14]. In addition, sliding mode control (SMC) has been widely employed to control FJMs systems due to its robustness against disturbances and parameter variations. To address some of the problems associated with classical SMC and further improve its performance, hybrid approaches combining SMC with fuzzy logic or observers have been proposed in [15]–[17]. Disturbance observer based and observer assisted sliding mode approaches have recently applied to FJM and shown an improved robustness and reduced sensitivity to uncertainties [18], [19].

Alongside controller design, parameter tuning remains an important part of the design challenge. Optimization algorithms such as particle swarm optimization (PSO) and genetic algorithms (GA) have been widely used to determine optimal controller parameters in complex nonlinear systems [20], [21]. Recent studies proposed a controller that combines PSO with advanced nonlinear control techniques to suppress vibration and enhance trajectory tracking characteristics [3], [22].

Most existing studies focus on single controller, without providing fair comparative evaluations under identical tuning, operating conditions, and test scenarios. In contrast, this paper presents a systematic comparative study between a cascaded FOPID controller and SMC for a 2DOF flexible joint manipulator. Both controllers are implemented using similar cascade framework and tuned using PSO with same settings and conditions to ensure a fair comparison. The main contribution of this work is to evaluate the trade-offs between tracking performance, robustness, and control consumed energy. Simulation results collected under nominal conditions, external disturbances, and variable payloads reveal that FOPID provides superior tracking accuracy and robustness, whereas SMC offers smoother actuator responses with lower control energy. These results provide practical guide to select suitable control scheme and determine the required actuators energy rating to be used in flexible robotic systems.

2. MATHEMATICAL MODELING OF 2DOF FJM

The dynamic equations of the 2DOF flexible joint manipulator, as shown in Figure 1, were obtained based on the rotational motion for each link. Due to the flexible joint structure, there are two separate dynamic equations for each joint: one for the link side and the other for the motor side. The variables used in the system are: θ_1, θ_2: link angles, θ_{m1}, θ_{m2}: motor angles, and u_1, u_2: motor input torques. The other system parameters used in the study are given in Table 1, assuming that both links are identical.

In real 2DOF robot systems, the movement of one joint affects the other. To include this effect in the model, the gravity terms are arranged as (1):

$$\begin{aligned} g_1 &= M_1 g L_1 [\sin(\theta_1) + \alpha \sin(\theta_1 + \theta_2)] \\ g_2 &= M_2 g L_2 \sin(\theta_1 + \theta_2) \end{aligned} \tag{1}$$

where α represents the coupling coefficient. Then, the link side dynamics can be expressed as (2).

$$\begin{aligned} \ddot{\theta}_1 &= -\frac{1}{I_1} g_1 - \frac{K_1}{I_1}(\theta_1 - \theta_{m1}) + \frac{1}{I_1} d_{L1} + \beta_1 \dot{\theta}_2 \\ \ddot{\theta}_2 &= -\frac{1}{I_2} g_2 - \frac{K_2}{I_2}(\theta_2 - \theta_{m2}) + \frac{1}{I_2} d_{L2} + \beta_2 \dot{\theta}_1 \end{aligned} \tag{2}$$

On the other side is the motor side dynamics which can be determined using (3).

$$\begin{aligned} \ddot{\theta}_{m1} &= \frac{K_1}{J_1}(\theta_1 - \theta_{m1}) + \frac{1}{J_1} u_1 \\ \ddot{\theta}_{m2} &= \frac{K_2}{J_2}(\theta_2 - \theta_{m2}) + \frac{1}{J_2} u_2 \end{aligned} \tag{3}$$

A feed forward gravity balancer is designed in the system to reduce the effect of gravity and improve control performance. Thanks to this structure, the controller is enabled to focus only on the tracking error. Gravity compensator control inputs are defined as (4):

$$\begin{aligned} u_1 &= K_1(\theta_1 - \theta_{m1}) + g_1 \\ u_2 &= K_2(\theta_2 - \theta_{m2}) + g_2 \end{aligned} \tag{4}$$

In this approach, the first term compensates for the flexible joint effect, while the second term compensates for the gravity effect. The resulting model takes into account flexible joint dynamics and coupling between links. In this way, it offers a more realistic structure in terms of both control design and system analysis. In particular, the inclusion of gravity coupling in the model provides a significant advantage in evaluating the performance of multivariate control algorithms.

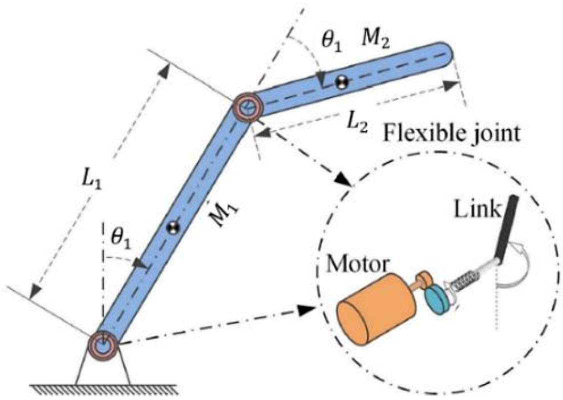

Figure 1. Two links flexible joint manipulator [23]

Table 1. Flexible joint manipulator parameters [24]

Parameter	Description	Value
M_1, M_2	Link mass	0.25 Kg
L_1, L_2	Link length	0.35 m
K_1, K_2	Joint spring constant	20 N·m/rad
I_1, I_2	Link moment of inertia	0.2 Kg.m^2
J_1, J_2	Motor moment of inertia	1 Kg.m^2
g	Gravitational acceleration	9.8 m/s^2
α	Gravitational coefficient	0.3 N·m/Kg
β_1, β_2	Velocity coupling coefficient	0.05 N·m·s./rad

3. CONTROLLER DESIGN

3.1. FOPID controller design

The FOPID controllers have more adjustable parameters compared to classical PID controllers. They offer a more flexible control performance, especially in nonlinear and coupled systems such as FJM systems, because the operators (λ, μ) provide additional degrees of freedom helping in cancel out flexible joint elasticities. In this section, the design details of FOPID are discussed. The output of controller based on the difference between the desired output and actual output. The time domain representation of FOPID is (5),

$$u_{fopid} = k_p e(t) + k_i \frac{d^{-\gamma} e(t)}{dt^{-\gamma}} + k_d \frac{d^{\delta} e(t)}{dt^{\delta}} \tag{5}$$

where k_p, k_i, and k_d denote the proportional gain, integral gain and derivative gain respectively. γ refers to the fractional integral scalar and δ refers to the fractional derivative scalar. $e(t)$ represents the error signal.

The proposed control architecture consists of two layers: Inner loop which will be responsible of controlling motor angles, while the outer loop controls link angles. Thus, the system includes four FOPID controllers in total. The purpose of the inner loop is to ensure that the motor angles follow the reference values quickly and steadily. In this loop, the error signal is defined as $e_m = \theta_{m,ref} - \theta_m$. The inner loop is critical to suppress the fast dynamics of the system and reduce oscillations caused by elasticity. The purpose of the outer loop is to bring the link angles to the desired reference values. The output produced in this loop is the reference motor angles for the inner loop, and the error signal in this loop is defined as $e = \theta_{ref} - \theta$. The decentralized cascade control structure can be scaled effectively to multi DOF industrial robots and collaborative systems (cobots). Splitting control actions into an inner loop and an outer loop, leads to the possibility of applying the controller independently on a joint-by-joint basis. In order to increase control performance, the FOPID controller structure is used together with the gravity stabilizer. In this case, the total control input is expressed as (6):

$$u_i = u_{FOPID,i} + u_{g,i}, \quad i = 1,2 \tag{6}$$

where $u_{FOPID,i}$ is the FOPID controller output, and $u_{g,i}$ is the gravity balancing term. Following this approach, the controller focuses only on the tracking error without having to compensate for the effect of gravity. This provides a significant performance increase, especially in systems where nonlinear effects dominate, while ensuring smooth control signals that prevent actuator thermal stress.

3.2. Lyapunov stability analysis of FOPID controller

In this section, the stability of the closed loop system under the FOPID controller is analyzed using Lyapunov approach. Consider the following positive definite Lyapunov function:

$$V_i = \frac{1}{2} e_i^2 \tag{7}$$

By taking the first derivative of (7):

$$\dot{V}_i = e_i \dot{e}_i \tag{8}$$

The FOPID controller generates a control action based on proportional, integral, and derivative terms:

$$u_i = k_{p,i} e_i + k_{i,i} D^{-\gamma_i} e_i + k_{d,i} D^{\delta_i} e_i \tag{9}$$

This control law acts to reduce both the error and its rate of change. With properly tuned controller gains, the proportional term reduces the instantaneous error while the fractional integral and the fractional derivative term eliminates steady state error and provides damping respectively. In this context, the control input ensures that $e_i \dot{e}_i < 0$, which implies $\dot{V}_i < 0$. Therefore, the error dynamics are stable in the sense of Lyapunov, and the tracking error converges toward zero.

3.3. Sliding mode controller design

Sliding mode controller (SMC) with boundary layer is employed as a comparison benchmark for more comprehensive evaluation of the proposed cascaded FOPID controller. Similar to the FOPID design, a cascade control architecture is employed where the outer loop is responsible for link position tracking. The sliding surface is defined as (10):

$$s_1 = e_2 + \lambda_{smc} e_1 \tag{10}$$

where $e_1 = \theta_{1,ref} - \theta_1$, $e_2 = \dot{\theta}_{1,ref} - \dot{\theta}_1$, and $\lambda_{smc} > 0$ is the sliding surface gain. A virtual acceleration input v_1 is designed as (11):

$$v_1 = \ddot{\theta}_{1,ref} - \lambda_{smc} e_2 - \gamma_{1,smc} \operatorname{sat}\left(\frac{s_1}{\phi_{1,smc}}\right) \tag{11}$$

Using the link side dynamics, the desired motor angle $\theta_{m1,ref}$ is obtained as (12):

$$\theta_{m1,ref} = \theta_1 + \frac{I_1 v_1 + M_1 g L_1 \sin(\theta_1)}{K_1} \tag{12}$$

The inner loop ensures that the motor angle tracks the reference generated by the outer loop. The sliding surface for the inner loop is defined as (13):

$$s_2 = \dot{e}_3 + c_{smc} e_3 \tag{13}$$

where $e_3 = \theta_{m1,ref} - \theta_{m1}$ is the motor tracking error, $\dot{e}_3 = \dot{\theta}_{m1,ref} - \dot{\theta}_{m1}$, and $c_{smc} > 0$. Then the control law which represents the motor torque input is designed as (14):

$$u_1 = -k_{p,smc} e_3 - k_{d,smc} \dot{e}_3 - \gamma_{2,smc} \operatorname{sat}\left(\frac{s_2}{\phi_{2,smc}}\right) \tag{14}$$

where $\phi_{1,smc}$ and $\phi_{2,smc}$ define the boundary layer thicknesses for the outer and inner loops, respectively. For the purpose of fair comparison, the proposed SMC is combined with gravity compensation similar to the FOPID structure:

$$u_i = u_{SMC,i} + u_{g,i}, i = 1,2 \quad (15)$$

where $u_{SMC,i}$ is sliding mode control input, and $u_{g,i} = K_i(\theta_i - \theta_{mi}) + g_i$

3.4. Parameter tuning with optimization algorithms

The FOPID cascade control structure proposed in this study includes a total of 20 adjustable parameters. Determining these parameters with classical methods is quite difficult and time consuming due to the nonlinear and coupled structure of the system. In this context, a particle swarm optimization (PSO) algorithm [25] is utilized to search the parameter space efficiently and close to global optima. Integral of absolute error (IAE) for the two links' angles were taken into consideration together in order to evaluate the control performance.

$$J = \int_0^T \mid e_{Link1}(t) \mid dt + \int_0^T \mid e_{Link2}(t) \mid dt \quad (16)$$

The operational PSO parameters used through the tuning process are swarm size of 40, 80 iterations, inertia weight of 0.9, and cognitive/social coefficients of 2. Based on these configurations, the final optimized controller parameters for both the FOPID and SMC frameworks are listed in Table 2.

4. SIMULATION RESULTS

To illustrate the effectiveness of the proposed controller, different scenarios have been done to check the ability of controller in trajectory tracking and in the existence of external disturbance and payload variations. The following performance metrics are used to evaluate controller performance: integral time absolute error (ITAE) evaluates transient performance quality, Steady state error measures tracking accuracy, $MP\%$ represents percentage maximum overshoot, Ts denotes settling time, Tr indicates rise time, and integral of squared control effort (ISCE) gives an indication on the energy consumed by the actuator.

Table 2. FOPID and SMC controllers tuned parameters

Parameters	FOPID				Parameters	SMC	
	FOPID (θ_1)		FOPID (θ_2)			SMC (θ_1)	SMC (θ_2)
	Outer	Inner	Outer	Inner			
K_p	56.939	92.698	49.281	86.163	λ_{smc}	6.3072	9.2285
K_i	11.854	1.3081	5.9034	1.5758	$\gamma_{1,smc}$	17.749	12.701
K_d	17.822	2.3204	2.9080	12.850	$\phi_{1,smc}$	0.5000	0.4679
λ	0.9909	1.5662	1.3871	1.1359	$k_{p,smc}$	61.116	43.543
μ	0.3487	1.6580	0.5361	1.2695	$k_{d,smc}$	2.4651	26.795
					$\gamma_{2,smc}$	5.3847	5.6455
					c_{smc}	6.9071	8.2392
					$\phi_{2,smc}$	0.0144	0.0284

4.1. Scenario 1: nominal system (no disturbance, no payload)

In the first test, the system was evaluated under ideal nominal conditions. A step reference of 0.5 rad was applied to link 1 at $t = 0$ s, and a 0.2 rad step was applied to link 2 at $t = 2$ s. Performance indices for both controllers are listed in Table 3. The links' angles responses and the actuators' responses are depicted in Figure 2 and Figure 3 respectively. The results reveal a clear difference in the transient behavior of the two controllers. For link 1, the SMC demonstrated an entirely damped response with 0% overshoot, whereas the FOPID controller exhibited an overshoot of 8.55%. Similar behavior was observed in link 2. However, FOPID achieved superior overall tracking accuracy, minimizing the ITAE error compared to SMC's. FOPID also maintained a tighter steady state error (0.0019) than SMC (0.0037). Most notably, the control effort (ISCE) where SMC expended significantly less energy compared to FOPID's highly aggressive control action.

As shown in Figures 3(a) and 3(b), the actuator signals associated with FOPID exhibit more fluctuations, explaining the high value of ISCE when compared with those of SMC. In practical robotic systems, high control activity leads to an increase in actuator power consumption and thermal stress, which can reduce actuator efficiency and require larger motor ratings.

Table 3. Performance indices for nominal system test (Scenario 1)

Performance metric	SMC (θ_1)	FOPID (θ_1)	SMC (θ_2)	FOPID (θ_2)
ITAE error	0.2423	0.1165	0.5749	0.1962
Steady state error	0.0037	0.0019	0.0077	0.0015
MP%	0	8.5529	0	9.23798
Ts	1.1973	0.9787	1.125	1.00369
Tr	0.5524	0.2291	0.5652	0.22936
ISCE	23.35	154.78	8.86	45.29

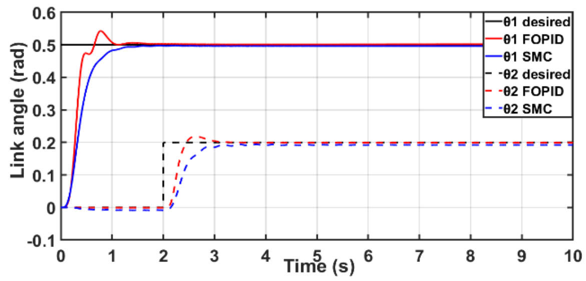

Figure 2. Link angle tracking responses of the nominal system

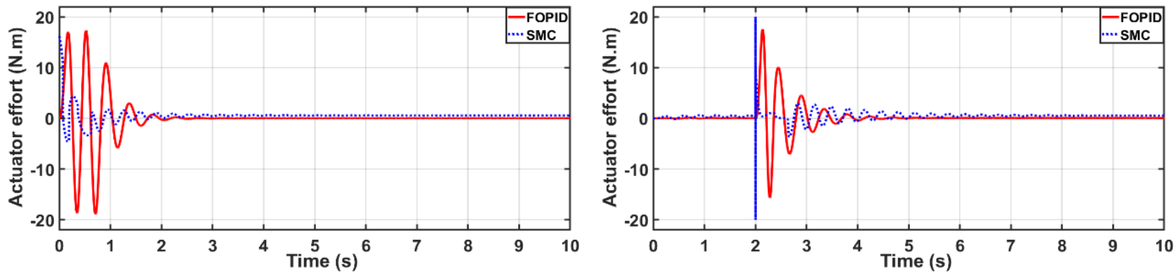

Figure 3. Control signal (actuator effort) under nominal system: (a) first link and (b) second link

4.2. Scenario 2: disturbance at link 1

To test disturbance rejection, external load perturbations were applied to the system. The complete link angle tracking responses and their corresponding control effort signals are shown in Figure 4 and Figure 5 respectively, while the performance indices values are listed in Table 4. First, a 0.5 N.m disturbance was injected at link 1 at $t = 5$ s. FOPID successfully suppressed the disturbance with negligible impact (Figure 4(a)), maintaining an ITAE of 0.1461. SMC showed a slight degradation in performance, with its ITAE increasing to 0.3793 and steady-state error rising to 0.0075 on link 1. The control effort for SMC slightly increased to 31.76 to compensate for the disturbance, accompanied by signal chattering in its actuator signal after $t = 5$ s while FOPID's effort remained high for both links as illustrated in Figures 5(a) and 5(b).

When the disturbance on link 1 was increased to 1.0 N.m at $t = 5$ s, the limitations of the SMC design became highly evident. As shown in the plotted responses in Figure 4(b) and the corresponding control signal behaviors in Figures 5(c) and 5(d), the SMC failed to suppress the disturbance, leading to severe chattering, continuous saturation in the actuator signal ($\pm 20\ N.m.$) and severe instability in link 1. The numerical results for this test in Table 4 clearly indicating the loss of tracking. Conversely, the FOPID controller exhibited remarkable robustness. Despite the severe 1.0N disturbance, it maintained stable tracking and in the same time kept the control effort smoothly damped within safe operational limits.

Table 4. Performance indices for disturbance tests (Scenario 2)

Performance metric	0.5 N.m disturbance				1.0 N.m disturbance			
	SMC (θ_1)	FOPID (θ_1)	SMC (θ_2)	FOPID (θ_2)	SMC (θ_1)	FOPID (θ_1)	SMC (θ_2)	FOPID (θ_2)
ITAE	0.3793	0.1461	0.5804	0.1962	39.44	0.178	0.8431	0.1962
Steady state error	0.0075	0.0022	0.0079	0.0015	Nan	0.0025	0.025	0.0015
ISCE	31.76	186.34	9.056	53.14	994.8	192.76	29.44	67.49

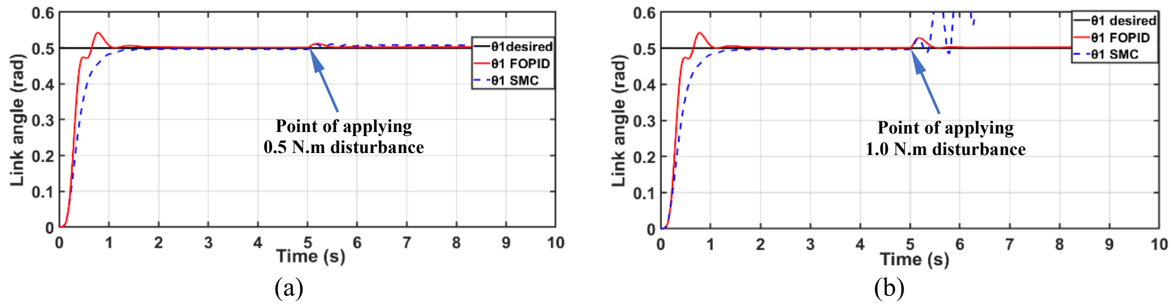

Figure 4. Link angle tracking responses under disturbance tests: (a) 0.5 N.m disturbance and (b) 1 N.m disturbance

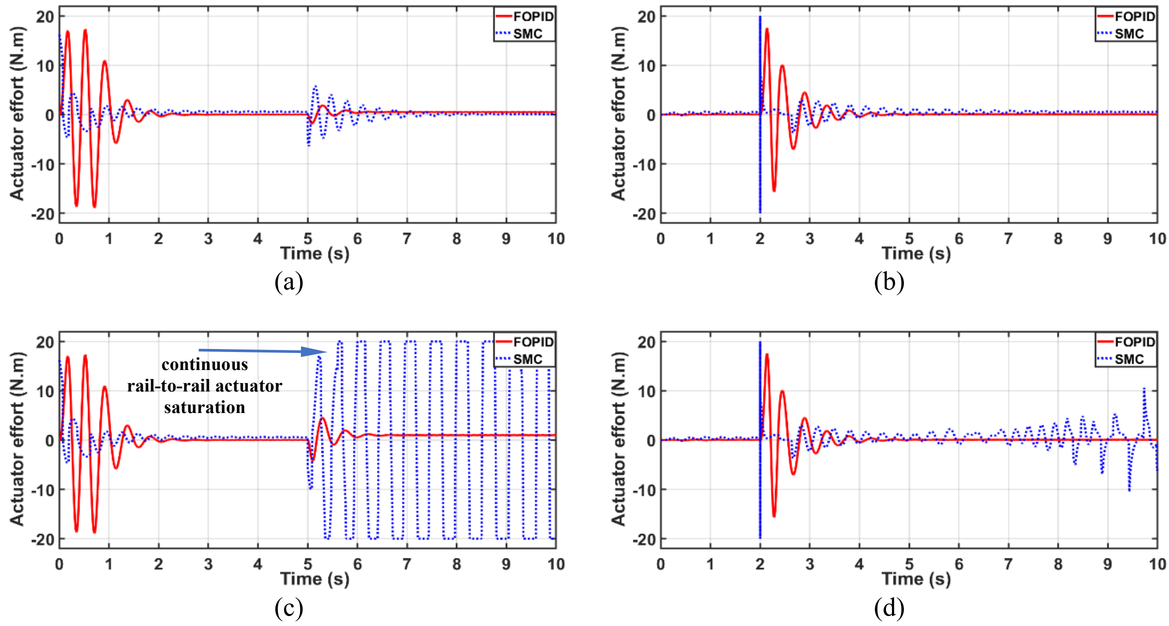

Figure 5. Control signal (actuator effort) under different external load disturbances (a) link 1 with 0.5 N.m, (b) link 2 with 0.5 N.m, (c) link 1 with 1.0 N·m, and (d) link 2 with 1.0 N.m

4.3. Scenario 3: variable payload

In the final scenario, the system was subjected to a variable payload, stepping to 0.1 kg at $t = 5$ s, and further to 0.3 kg at $t = 7$ s. As shown in Figure 6, both controllers successfully adapted to the parametric variations without losing stability. FOPID once again provided superior tracking, keeping the ITAE on link 1 at 0.1082. SMC handled the payload changes adequately but resulted in higher tracking deviations as shown in Table 5. Control effort shown in Figure 7 followed the established trend, with SMC operating efficiently versus FOPID's heavy energy usage. For both links, SMC introduces high frequency chattering reactions at the payload transition points ($t = 5$ s) and ($t = 7$ s) as shown in Figures 7(a) and 7(b). Overall, the total energy metrics in Table 6 show that SMC operating with lower cumulative numerical indices versus FOPID's higher energy usage. To illustrate the actuator energy requirements of both controllers, Figure 8 presents the ISCE values obtained under all the above scenarios. It can be observed that the SMC generally requires lower control energy compared to FOPID under all tests.

Table 5. Performance indices for payload variation test (Scenario 3).

Performance metric	Theta 1 SMC	Theta 1 FOPID	Theta 2 SMC	Theta 2 FOPID
ITAE	0.6746	0.1082	0.9587	0.2353
Steady state error	0.019	0.0014	0.02	0.0021
ISCE	35.95	192.76	25.88	54.71

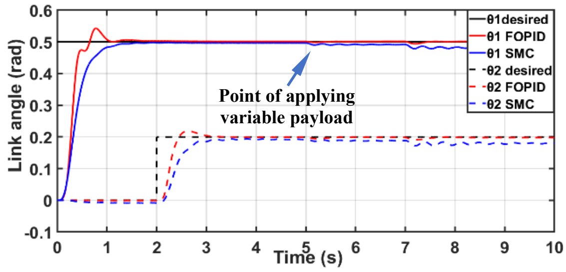

Figure 6. Link angle tracking responses under payload variations

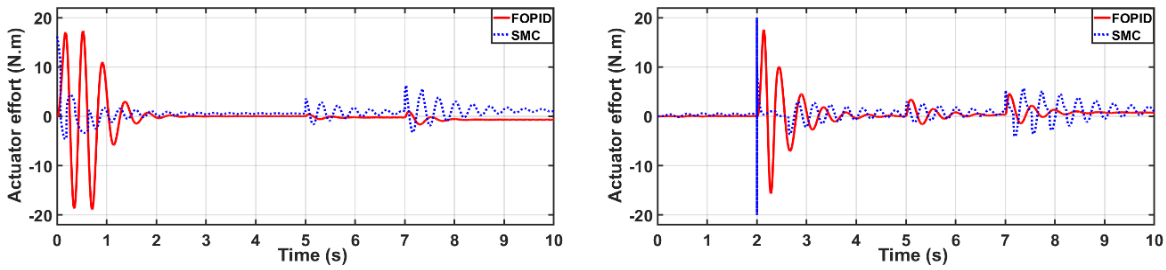

(a) (b)

Figure 7. Control signal (actuator effort) under payload variation (a) first link, (b) second link

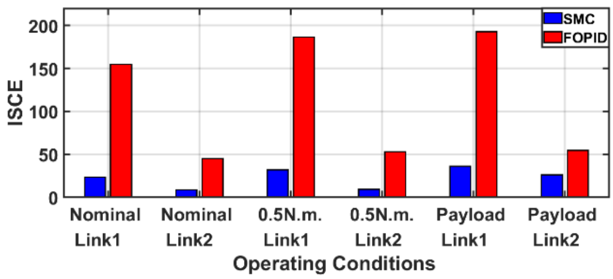

Figure 8. Comparison of actuator effort (ISCE) under different operating conditions

5. CONCLUSION

The main novelty of this work is a fair comparative evaluation between cascaded FOPID and SMC controllers applied to flexible joint manipulator. Both controllers were provided with gravity compensator and tuned under identical conditions using PSO and examined under identical conditions to ensure fair assessment. Three different simulation scenarios were conducted revealing a practically significant trade-off. Under nominal conditions, SMC provided smooth, zero overshoot transient responses with lower control effort, making it suitable for energy saving applications in controlled environments. However, when subjected to a relatively high external disturbance, SMC exhibited severe chattering and instability, whereas FOPID maintained stable and accurate tracking, demonstrating high robustness. Similar superiority was observed under variable payload conditions, where FOPID achieved lower ITAE and steady state errors across both links. In conclusion, SMC is the preferred choice for applications where energy efficiency and smooth transient behavior are of high priority. The reduced control effort of SMC decreases actuator heating and improves its efficiency in practical implementations. FOPID is the superior choice for environments subject to heavy, unpredictable disturbances and dynamic payload variations, provided the actuators can safely supply its high energy demands.

Since flexible joint manipulators rely heavily on sensor feedback, sensor accuracy has a large impact on system performance. Measurement noise mainly affects derivative and switching control actions and, in this context, SMC is generally more sensitive to sensor noise due to its associated switching action, whereas FOPID provides smoother control signals. Sensor delay may also cause reduction in stability margins and could lead to an increase in settling time, particularly during fast trajectory tracking. In practical systems, these effects can be reduced using filtering techniques, or high-resolution encoders. Both controllers can be implemented using standard real time platforms such as DSP or FPGA controllers. The required computations mainly include simple algebraic calculations and fractional order approximations, making real time implementation suitable for industrial robotic applications. It is worth to mention that both controllers are designed with hardware in the loop deployment in mind. Future work will investigate experimental validation of the proposed cascaded FOPID controller on a physical flexible joint platform.

FUNDING INFORMATION

Authors receive no funding.

AUTHOR CONTRIBUTIONS STATEMENT

This journal uses the Contributor Roles Taxonomy (CRediT) to recognize individual author contributions, reduce authorship disputes, and facilitate collaboration.

Name of Author	C	M	So	Va	Fo	I	R	D	O	E	Vi	Su	P	Fu
Ahmed Alkamachi	✓		✓		✓	✓	✓			✓	✓			✓
Ali Hussien Mary		✓	✓	✓				✓	✓			✓	✓	

C : **C**onceptualization
M : **M**ethodology
So : **So**ftware
Va : **Va**lidation
Fo : **Fo**rmal analysis
I : **I**nvestigation
R : **R**esources
D : **D**ata Curation
O : Writing - **O**riginal Draft
E : Writing - Review & **E**diting
Vi : **Vi**sualization
Su : **Su**pervision
P : **P**roject administration
Fu : **Fu**nding acquisition

CONFLICT OF INTEREST STATEMENT

Authors state no conflict of interest.

DATA AVAILABILITY

The data that support the findings of this study are available from the corresponding author upon reasonable request. The simulation models and parameters used in this study are provided within the manuscript.

REFERENCES

[1] Y. Chen and B. Guo, “Sliding mode fault tolerant tracking control for a single-link flexible joint manipulator system,” *IEEE Access*, vol. 7, pp. 83046–83057, 2019, doi: 10.1109/ACCESS.2019.2923789.

[2] S. Sampath, P. Duraisamy, A. M., A. Karthikeyan, and K. Rajagopal, “Effect of nonlinear stiffness on single link flexible joint robotic manipulator and its control,” *International Journal of Non-Linear Mechanics*, vol. 163, p. 104730, Jul. 2024, doi: 10.1016/j.ijnonlinmec.2024.104730.

[3] Y. Guan, Y. Wang, R. Yin, M. Chen, and Y. Xu, “Vibration suppression and trajectory tracking control of flexible joint manipulator based on PSO algorithm and fixed-time control,” *International Journal of Intelligent Systems*, vol. 2024, pp. 1–23, Jun. 2024, doi: 10.1155/2024/5510259.

[4] S. Kizir, Z. Bingul, and J. T. Agee, “Point-to-point virtual model control of a flexible joint robotic manipulator using trajectories of motion,” *Transactions of the Institute of Measurement and Control*, vol. 47, no. 4, pp. 623–633, Feb. 2025, doi: 10.1177/01423312241254871.

[5] A. H. Mary, T. Kara, and A. H. Miry, “Inverse kinematics solution for robotic manipulators based on fuzzy logic and PD control,” in *2016 Al-Sadeq International Conference on Multidisciplinary in IT and Communication Science and Applications (AIC-MITCSA)*, May 2016, pp. 1–6. doi: 10.1109/AIC-MITCSA.2016.7759929.

[6] K. Ibrahim and A. B. Sharkawy, “A hybrid PID control scheme for flexible joint manipulators and a comparison with sliding mode control,” *Ain Shams Engineering Journal*, vol. 9, no. 4, pp. 3451–3457, Dec. 2018, doi: 10.1016/j.asej.2018.01.004.

[7] H.-M. Yen, T.-H. S. Li, and Y.-C. Chang, “Adaptive neural network based tracking control for electrically driven flexible-joint robots without velocity measurements,” *Computers & Mathematics with Applications*, vol. 64, no. 5, pp. 1022–1032, Sep. 2012, doi: 10.1016/j.camwa.2012.03.020.

[8] Sung Jin Yoo, Jin Bae Park, and Yoon Ho Choi, “Adaptive output feedback control of flexible-joint robots using neural networks: dynamic surface design approach,” *IEEE Transactions on Neural Networks*, vol. 19, no. 10, pp. 1712–1726, Oct. 2008, doi: 10.1109/TNN.2008.2001266.

[9] V.-T. Ngo and Y.-C. Liu, “On tracking control of robot manipulator with flexible joints in operational space,” *IFAC-PapersOnLine*, vol. 56, no. 2, pp. 1307–1312, 2023, doi: 10.1016/j.ifacol.2023.10.1770.

[10] R. Qi, H.-K. Lam, J. Liu, and J. Yu, “Adaptive fuzzy finite-time singular perturbation control for flexible joint manipulators with state constraints,” *IEEE Transactions on Systems, Man, and Cybernetics: Systems*, vol. 54, no. 12, pp. 7521–7527, Dec. 2024, doi: 10.1109/TSMC.2024.3446172.

[11] D. Pavlichenko and S. Behnke, "Flexible-joint manipulator trajectory tracking with learned two-stage model employing one-step future prediction," in *2021 Fifth IEEE International Conference on Robotic Computing (IRC)*, Nov. 2021, pp. 1–9. doi: 10.1109/IRC52146.2021.00008.

[12] B. Niu and H. Zhang, "Linear parameter-varying modeling for gain-scheduling robust control synthesis of flexible joint industrial robot," *Procedia Engineering*, vol. 41, pp. 838–845, 2012, doi: 10.1016/j.proeng.2012.07.252.

[13] R. Datta, R. Dey, and N. Adhikari, "Dissipative control for single flexible joint robotic system via T–S fuzzy modelling approach," *IFAC-PapersOnLine*, vol. 55, no. 1, pp. 637–642, 2022, doi: 10.1016/j.ifacol.2022.04.104.

[14] J. Han, X. Shan, H. Liu, J. Xiao, and T. Huang, "Fuzzy gain scheduling PID control of a hybrid robot based on dynamic characteristics," *Mechanism and Machine Theory*, vol. 184, p. 105283, Jun. 2023, doi: 10.1016/j.mechmachtheory.2023.105283.

[15] D. Shang, X. Li, M. Yin, and F. Li, "Dynamic modeling and fuzzy adaptive control strategy for space flexible robotic arm considering joint flexibility based on improved sliding mode controller," *Advances in Space Research*, vol. 70, no. 11, pp. 3520–3539, Dec. 2022, doi: 10.1016/j.asr.2022.08.042.

[16] D. Shang, X. Li, M. Yin, and F. Li, "Dynamic modeling and fuzzy compensation sliding mode control for flexible manipulator servo system," *Applied Mathematical Modelling*, vol. 107, pp. 530–556, Jul. 2022, doi: 10.1016/j.apm.2022.02.035.

[17] S. Zaare and M. R. Soltanpour, "Continuous fuzzy nonsingular terminal sliding mode control of flexible joints robot manipulators based on nonlinear finite time observer in the presence of matched and mismatched uncertainties," *Journal of the Franklin Institute*, vol. 357, no. 11, pp. 6539–6570, Jul. 2020, doi: 10.1016/j.jfranklin.2020.04.001.

[18] Z. Yan, X. Lai, Q. Meng, J. She, and M. Wu, "Time-varying disturbance-observer-based tracking control of uncertain flexible-joint manipulator," *Control Engineering Practice*, vol. 139, p. 105624, Oct. 2023, doi: 10.1016/j.conengprac.2023.105624.

[19] A. Sharma and S. Janardhanan, "Position control of single-link flexible manipulator: a functional observer based sliding mode approach," in *2024 European Control Conference (ECC)*, Jun. 2024, pp. 3684–3689. doi: 10.23919/ECC64448.2024.10590997.

[20] A. H. Miry, A. H. Mary, and M. H. Miry, "Improving of maximum power point tracking for photovoltaic systems based on swarm optimization techniques," *IOP Conference Series: Materials Science and Engineering*, vol. 518, no. 4, p. 042003, May 2019, doi: 10.1088/1757-899X/518/4/042003.

[21] B. A. Tawfeeq, M. Y. Salloom, and A. Alkamachi, "A self-balancing platform on a mobile car," *International Journal of Electrical and Computer Engineering (IJECE)*, vol. 12, no. 6, p. 5911, Dec. 2022, doi: 10.11591/ijece.v12i6.pp5911-5922.

[22] O. Karahan and H. Karci, "Design of robust fractional order fuzzy PID sliding mode controller based on hybrid swarm intelligence algorithm for a 6-DOF robotic manipulator," *Robotica*, vol. 43, no. 3, pp. 1110–1139, Mar. 2025, doi: 10.1017/S0263574725000141.

[23] X. Cheng, H. Liu, and W. Lu, "Chattering-suppressed sliding mode control for flexible-joint robot manipulators," *Actuators*, vol. 10, no. 11, p. 288, Oct. 2021, doi: 10.3390/act10110288.

[24] X. C. Nguyen and D. T. Le, "Adaptive finite-time synergetic control for flexible-joint robot manipulator with disturbance inputs," *Electrical Engineering & Electromechanics*, no. 3, pp. 45–52, May 2025, doi: 10.20998/2074-272X.2025.3.07.

[25] J. Fu, S. Gu, L. Wu, N. Wang, L. Lin, and Z. Chen, "Research on optimization of diesel engine speed control based on UKF-filtered data and PSO fuzzy PID control," *Processes*, vol. 13, no. 3, p. 777, Mar. 2025, doi: 10.3390/pr13030777.

BIOGRAPHIES OF AUTHORS

Ahmed Alkamachi received his Ph.D. degree in control engineering and is currently working as an Assistant Professor in the Department of Mechatronics Engineering at the University of Baghdad, Iraq. His research interests include control systems, system modelling, robotics, nonlinear control, unmanned aerial vehicles (UAVs), and optimization techniques. He has contributed to several research works in the fields of advanced control strategies and intelligent optimization methods for nonlinear and complex engineering systems. He can be contacted at ahmed78@kecbu.uobaghdad.edu.iq.

Ali Hussien Mary received the B.Sc. and M.Sc. degrees in electrical engineering from the College of Engineering, University of Baghdad, Baghdad, Iraq. In 1998 and 2001 respectively. He obtained his Ph.D. degree in electrical engineering from Gaziantep University, Turkey, in 2017. He is currently a Full Professor at Al-Khwarizmi College of Engineering, University of Baghdad. His research interests include control systems, robotics, and artificial intelligence. He has contributed to various academic and research activities in these fields, with a focus on advanced control techniques and intelligent systems. He can be contacted at alimary76@kecbu.uobaghdad.edu.iq.